Project closing report

Title: Exploring the impact of nanoparticles on productivity, metal uptake and iron metabolism of plants

Consortium project numbers: K115784, K115913

Project duration: 2016.01.01 - 2020.12.27

Introduction

Research of the preparation routes, peculiar properties and possible applications of nanoparticles is currently one of the main focus of natural sciences. In this diverse field, our interdisciplinary research project set out to investigate two lesser known sides of nanoparticles: their potential use as fertilizers useful to resolve or alleviate problems of agricultural crop production related to micronutrient constraints, and the potentially unfavourable effects exerted on plants by nanoparticles that may eventually also be released from the industry and consumer products to the environment.

Iron is one of the most important transition metal nutrients required by the healthy development of plants, and consequently its deficiency is one of the most limiting factors of plant biomass production. In addition, as plants also represent the major iron source in human nutrition, iron deficiency or disturbed iron homeostasis of plants also entails one of the most prevalent nutritional challenges for the world's population. Iron-based nanoparticles are therefore especially important as being potentially beneficial to ecosystems involving plants. In addition to iron, in calcareous and alkaline soils micronutrient constraints related especially to manganese and zinc are regarded as the most serious nutritional problems for plants.

In order to elucidate the beneficial and/or harmful effects of nanoparticles on plants in a meaningful manner, the nature of the nanoparticles applied in the experiments must be known with sufficient detail, including information on their composition, particle size, morphological, structural as well as magnetic and chemical properties. Furthermore, the control over these properties needs to be preferably achieved, by finding and applying custom preparation routes to produce nanomaterials with specific desired attributes. The implementation of our research project therefore required an interdisciplinary approach, which was realized in the form of a consortium covering on the one hand nanoparticle sample preparation and characterization (mainly in the frame of K115784), and on the other hand plant biological studies (K115913).

Events influencing the implementation of the project

Due to unforeseen events occurring in the initial host institution (Research Center of Natural Sciences, Hungarian Academy of Sciences) of the consortional project part K115784, during the first year of our project term a change in the host institution of K115784 had to be effected, and consequently starting with 2017 the implementation of this project part was continued in the Centre for Energy Research, Hungarian Academy of Sciences. Simultaneously with this change, from the originally altogether five participant researchers of K115784 two former participants could not continue their work on the project anymore, and two further participants had to reduce the intensity (FTE) of their participation for the rest of the project term. At the same time, five researchers newly joined the project as participant in the fields of nanoparticle sample preparation and characterization. As a result, starting with 2017 the total yearly FTE value of the participants of K115784 increased from the original 1.2 to 1.4.

At the end of 2019 the consortium was granted an extension of the original project term until 30th of June, 2020, which was later on further extended due to the COVID 19 pandemic finally until 27th of December, 2020.

Nanoparticles considered for plant biological studies

Given the particular importance of iron in the physiological processes of healthy plant development, concerning the preparation and characterization of nanoparticles to be applied in plant biological studies we focused our attention

mainly towards nanoparticles containing iron. We successfully prepared and characterized nanoparticles of FeCo alloy [1], $Mn_{0.25}Zn_{0.75}Fe_2O_4$ (in the form of colloid suspension later referred to as "**MSZ26**", Figure 1.a) and $Mn_{0.5}Zn_{0.5}Fe_2O_4$ [2], several different ferrihydrite/hematite nanoparticle suspensions by using different surfactants (in the followings referred to as „**FH**" for ferrihydrite, as in Figure 1.b, and „**NH**" for hematite, as in Figure 1.c) [3], a ferrihydrite/hematite/goethite nanoparticle suspension prepared by using metallic iron enriched in ^{57}Fe as the starting material (referred to as „**^{57}Fe-NH**", Figure 1.d), magnetite/maghemite nanoparticle powder samples with or without coating agent under different experimental conditions [4,5,6,7,8], nominally $ZnFe_2O_4$ nanoparticle powders with different crystallinity [9] as well as Fe/FeO nanoparticle powder composites by using electric wire explosion of bcc-iron wire [10].

In order to characterize the different nanoparticle samples we mainly applied suitable methods selected among transmission electron microscopy (TEM), selected area electron diffraction (SAED), energy-dispersive X-ray spectroscopy (EDS), scanning electron microscopy (SEM), powder X-ray diffractometry (PXRD), inductively coupled plasma optical emission spectrometry (ICP-OES), inductively coupled plasma mass spectrometry (ICP-MS), ^{57}Fe Mössbauer spectroscopy (^{57}Fe MS) and electron paramagnetic resonance / electron magnetic resonance spectroscopy (EPR / EMR).

Two separate Fe_xCo_{1-x} alloy nanoparticle samples were synthesized via wet-chemical redox synthesis from iron(III) chloride hexahydrate and cobalt(II) acetate as precursors along with aluminum powder and ammonium fluoride applied as reducing agents [1]. We have shown that the applied preparation method yields bcc alloy samples that are in a fully disordered (A2) atomic state, where the *a* and *b* sites of the bcc lattice are taken by iron (or cobalt) in equal proportions. The iron concentration of the samples was successfully determined on the basis of the analysis of EDS, ICP-MS and ^{57}Fe MS measurements. The nanoparticle powder sample subsequently used in plant biological studies (denoted further on as „**nanoFeCo**") was a nearly equiatomic alloy, characterized as $Fe_{0.53}Co_{0.47}$, with a mean crystallite size of ~ 24 nm.

$(Mn_xZn_{1-x})Fe_2O_4$ ferrites with $x = 0.25$ and 0.5 were obtained in the form of colloid suspension and dried powder as described in [11]. The colloids were studied by TEM and EMR, whereas the corresponding dried powder was measured with XRD, which latter confirmed the spinel ferrite structure of the particles. For $x = 0.25$, TEM revealed a particle size of ca. 5-10 nm (Figure 1.a), whereas the particles were somewhat larger (around 10 nm) in the case of $x = 0.5$. The application of this sample is particularly interesting, because it incorporates in a single compound three different micronutrient metals (Mn, Zn, Fe) whose constraints can present nutritional problems for plants in calcareous and alkaline soils.

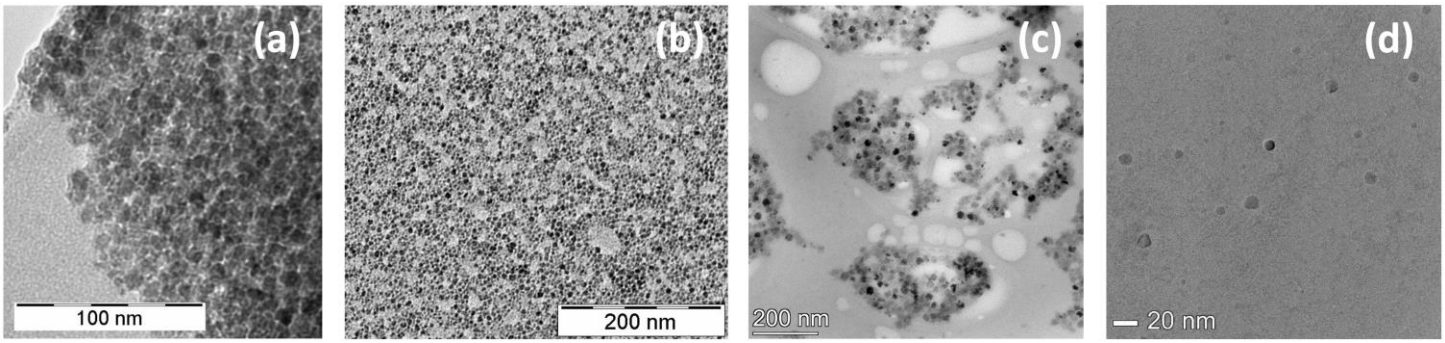

Figure 1. Examples of TEM images of nanoparticles prepared in the form of nanocolloid suspensions: (a) $(Mn_{0.25}Zn_{0.75})Fe_2O_4$ nanoparticles ("MSZ26"), (b) ferrihydrite nanoparticles ("FH"), (c) hematite nanoparticles ("NH", with a particle size typically below 20 nm), (d) iron oxide / iron oxide hydroxide nanoparticles enriched in ^{57}Fe, with a diameter of 4-12 nm („^{57}Fe-NH").

Preparation of ferrihydrite/hematite nanocolloid suspensions was based on a forced hydrolysis process, starting with 30 ml solution of 1% surfactant (e.g. polyethylene glycol) being administered to 600 ml deionized water at 80 °C. A volume of 50 ml solution of 0.5 M $FeCl_3 \times 6H_2O$ previously prepared was then added to the obtained surfactant solution with a rate of 2 ml min^{-1}, with an additional 2 hours of stirring at 80 °C. By using different surfactants (polyethylene glycols „Priowax 200" and „PEG 1500", polyoxyethylene ester of 12-hydroxystearic acid "LAB-236/2", and polyoxyethylene polyoxypropilane copolimer "Emulson 104/D") the resulted colloid suspensions contained different

ratios of ferrihydrite and hematite nanoparticles, as revealed by TEM measurements. The samples prepared with polyethylene glycols included ferrihydrite nanoparticles with a mean particle size of ca. 5 nm [3] (Figure 1.b), whereas larger (with a diameter of typically 10-20 nm, up to ca. 25 nm) hematite nanoparticles appeared in the samples prepared with the remaining surfactants. The concentration of nanoparticles could be fourfold increased in the ferrihydrite suspension prepared with „Priowax 200" by evaporation under vacuum, which resulted in a suspension with pH ≈ 1.5. In the latter sample a tendency of transformation of ferrihydrite to hematite was detected with a ferrihydrite half-conversion time of ca. 1.3 years.

An analogous sample (referred to as „**^{57}Fe-NH**") has been prepared from iron enriched in ^{57}Fe. TEM confirmed the presence of iron oxide / iron oxide hydroxide nanoparticles with a diameter of 4-12 nm in the sample (Figure 1.d), whereas on the basis of ^{57}Fe MS measurements the sample includes ferrihydrite, goethite and hematite, along with an Fe(II) component associated with dissolved iron.

Magnetite nanoparticles are prone to oxidation and consequently to a—partial or full—transformation to maghemite. We have studied the effects of preparation conditions [5,8], as well as the effect of carboxylic acid coating agents [4,6,7,8] on this oxidation process. We found that different carboxylic acids can promote either the oxidation or reduction of the as prepared iron oxide nanoparticles. We proposed and applied a novel method to decompose the heavily broadened room-temperature ^{57}Fe Mössbauer spectra of non-stoichiometric magnetite nanoparticles into signals of intermediate valence $Fe^{2.5+}$ and that of Fe^{3+} iron species [8]. We also proposed and applied a formula for the consideration of the room-temperature isomer shift value associated with the intermediate valence iron component in the estimation of the samples' formal Fe^{2+}/Fe^{3+} ratio, and revealed a correlation between the ratio in question and the cubic lattice parameter associated with the different nanoparticle samples. We have also demonstrated the ability of EMR spectroscopy to reflect oxidation-born deviations from the ideal magnetite stoichiometry in nanoparticle samples of non-stoichiometric magnetite [8].

The Fe_3O_4 nanoparticle powders „**MG001**" and „**MG002**" finally used in plant biological experiments were prepared, similarly to analogous samples studied in [8], via chemical co-precipitation method starting from mixed solution of Fe^{2+} and Fe^{3+} salts in strongly alkaline aqueous medium. $FeSO_4 \cdot 7H_2O$ and $FeCl_3 \cdot 6H_2O$ were used as metal precursors and KOH for pH adjustment in starting solutions. In the case of MG002 „Dextran 40000" was added to the solution as excipient, which—in comparison with MG001—appeared to promote the formation of smaller nanoparticle fractions. The particle size of these samples mainly covers the range of 5-10 nm (Figure 2), with some larger (up to ca. 20 nm in diameter) particles occurring as well. From XRD the crystallite size is ca. 11 nm, with the cubic lattice parameter (ca. 0.836 nm) referring to partial oxidation of magnetite in both cases.

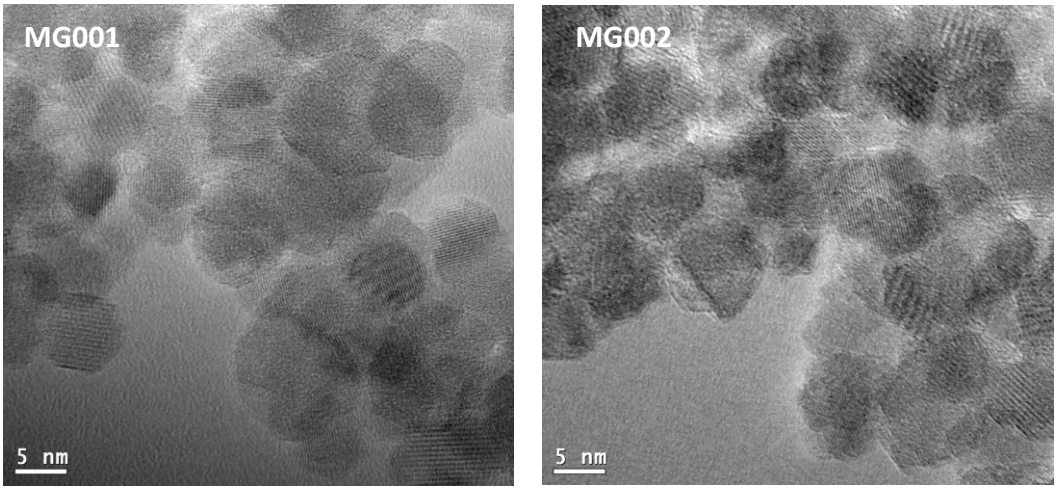

Figure 2. Excerpts of TEM images of "MG001" (left) and "MG002" (right) nanoparticle powder samples used in plant biological studies.

Two different Zn-ferrite spinel nanoparticle powder samples, in the following denoted with "**ZnFe001**" and "**ZnFe002**", were prepared via coprecipitation process according to the nominal stoichiometry of $ZnFe_2O_4$, from a mixed solution of

stoichiometric amounts of $ZnSO_4 \cdot 7H_2O$ and $FeCl_3$ $6H_2O$. Precipitation was achived via KOH solution at pH values of 11 ("ZnFe001") and 8 ("ZnFe002"). We performed a detailed characterization of the samples [9], which revealed that they both consist of roughly isometric spinel oxide nanoparticles with a characteristic size of ca. 5 nm, with the main difference between them being in the level of crystallinity. While the mean crystallite size (revealed by XRD) was roughly equal to the particle size in the case of "ZnFe001", it was in the order of ca. 1.6 nm for "ZnFe002".

The method of electric wire explosion (EWE) was applied to obtain iron bearing nanoparticles from bcc-Fe wire [10]. The process involves vaporization of thin iron wire in distilled water via electric discharge. Particles of a wide size distribution are produced (Figure 3a), with the smallest ones (fine fraction) forming a suspension. By the means of ^{57}Fe MS and XRD it was shown that the resulted product contained iron in particles of bcc-Fe and non-stoichiometric wüstite ($Fe_{1-x}O$, $x \approx 0.1$). For plant biological studies subsequently an analogous sample was prepared. By filtering the as-prepared suspension through filter paper, the latter retained a large part of the fine fraction of the particles, which fraction is referred to in the followings as "Fe-EWE-2018/S". ^{57}Fe MS revealed that this fraction is composed mainly of bcc-Fe (incorporating ca. 27% of the iron atoms in the sample) and non-stoichiometric wüstite. According to TEM, a fraction of the nanoparticles present in the sample displays a size well below 100 nm (Figure 3b). On the basis of SAED some of the smallest particles could be identified as magnetite. Following filtration, the produced water-clear filtered suspension (referred to as "Fe-EWE-2018/F") was further studied via TEM and ICP-OES, and was still found to include iron oxide nanoparticles and an overall iron concentration of 0.067 mg/l.

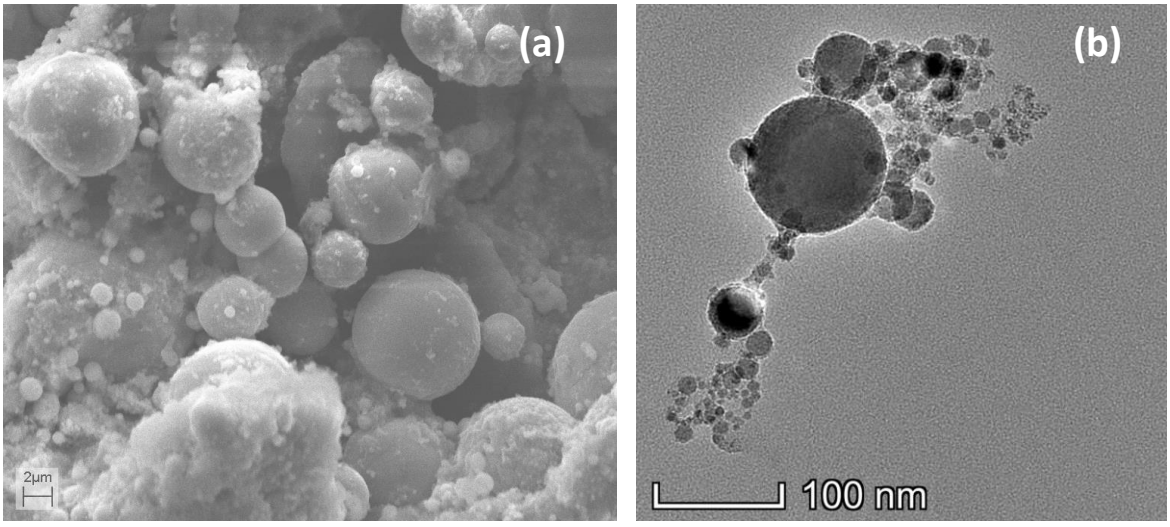

Figure 3. Excerpt of (a) a typical SEM image of the fine fraction of particles produced from bcc-Fe wire via EWE in water, and (b) TEM image of nanoparticle fractions of the sample "Fe-EWE-2018/S" (paper-bound Fe/FeO nanoparticles).

In addition, nanocolloid suspensions TiO_2 (referred to as „**nanoTiO_2**") and aluminium-hydroxide (referred to as "**ALH**") were applied in plant biological studies, and further nanoparticle samples prepared with or without iron, including nanometric goethite powder, nanometric $Mg(OH)_2$ powder and ZnO powder with a particle size in the submicron range were characterized as well. Furthermore, commercially purchased Al_2O_3 and ZnO nanoparticle powders were assessed to determine their suitability for subsequent biological studies. The nanosized iron-oxide-hydroxide core of a commercially purchased ferritin pharmaceutical analogue was investigated in detail [12], too. In the latter case, on the basis of TEM the size distribution of the iron-oxide-hydroxide cores were determined revealing that the diameter of core particles is typically smaller than 10 nm, with particle diameters around ca. 5 nm occurring most frequently.

Application of nanoparticles in plant biological studies

Natural form of iron in the applied plant model system

Iron may accumulate in various chemical forms during its uptake and assimilation in roots. Information on the permanent and transient Fe microenvironments formed during these processes in the Strategy I model plant cucumber

(Cucumis sativus L. cv. Joker F1) is important for studies addressing the Fe forms originating from any other treatments, including treatments with nanomaterials.

^{57}Fe Mössbauer spectroscopy and immunoblotting techniques were used to identify Fe microenvironments in plants supplied with ^{57}Fe(III)-citrate [13]. Reductive washing and high-resolution microscopy was applied to study the Fe localization. In the apoplast and on the root surface, transient presence of removable Fe-carboxylates and partly removable, amorphous hydrous ferric oxide/hydroxide in the nanoscale range, result of bacterial activity, have been identified respectively. At the same time, no ferritin accumulation was confirmed. In plants grown under Fe deficiency, the transient presence of highly soluble ferrous hexaaqua complex and the accumulation of Fe-carboxylates, likely Fe-citrate, were indicated. Being a non-removable compound, as major site of ^{57}Fe(III)-citrate accumulation the root xylem was suggested. When ^{57}Fe(III)-EDTA or ^{57}Fe(III)-EDDHA were applied as Fe-source, the higher soluble ferrous Fe accumulation was accompanied by a lower total Fe content. Results implicated, that chelates are more efficient in keeping Fe soluble, while less stable complexes as Fe(III)-citrate contribute better to Fe accumulation.

Utilization of iron from the nanoparticles of NH and ^{57}Fe-NH

Iron nutrition of plants depends on the utilization of Fe(III) containing soil minerals such as hematite. Although regeneration of plants from Fe deficiency is widely studied, mobilization of Fe from soil modelling particles is poorly characterized. Thus, we applied the colloid suspension samples NH (Figure 1.c) and ^{57}Fe-NH (Figure 1.d) to study the utilization of Fe from the nanomaterial particles in the frame of recovery treatments of cucumber showing iron deficiency symptoms.

Dissolution of NH was tested at pH 5.0. Overnight high speed centrifugation of the diluted nanocolloid suspension resulted in a significant pelleting, that fraction represented most of the Fe content of the material. The supernatant, indeed, contained a measurable amount of Fe.

The utilization of Fe from the nanomaterial particles was studied using cucumber, by TEM and ^{57}Fe Mössbauer spectroscopy in conjunction with the restoration of the iron deficiency responses [14]. Cucumber plants were grown under complete retraction of Fe in order to curtail any apoplast contamination with residual Fe which can supposedly affect the parameters studied. Iron deficient cucumber plants were treated with NH in 20 μM nominal concentration for Fe for one week. Electron microscopy analysis of root sections revealed dense particles in ultrathin sections across the root tip meristem, specifically in the middle lamella between the adjacent cell walls. Their diameter was comparable with but smaller than that of the original nanoparticles in the applied suspension. They often accumulated at the interfaces of the middle lamella and the adjacent walls, but also often formed groups and rows in the middle lamella itself, especially at the cell corners. Based on SPAD (Chlorophyll Meter) data, monitoring the relative chlorophyll abundance in leaves, the application of NH restored Fe chlorosis in three days treatment considerably.

Low temperature (T = 80 K) ^{57}Fe Mössbauer measurements of the iron deficient cucumber root, supplied with ^{57}Fe-NH colloid suspension of nominal Fe concentration of 100 μM for *one week*, demonstrated the presence of two magnetic sextets and a quadrupole doublet in the spectrum. The sextets have close hyperfine parameters to the ones found in the spectrum of the initial suspension. Therefore, these components probably correspond to the original nanoparticles of hematite and goethite. The Fe(III) doublet has higher relative area (67%) than in the initial colloid suspension spectrum (41%). Beside ferrihydrite particles attached to the roots, this component may therefore also be associated with iron that was taken up during the treatment period. However, the observed difference may also indicate that the relative occurrence of iron in the form of ferrihydrite is higher in the roots than in the original suspension. Fe(II) components were not observed in the Mössbauer spectrum of the roots.

In the ^{57}Fe Mössbauer spectrum of roots of iron deficient plants supplied with 57Fe-NH suspension of nominal Fe concentration of 100 μM for *30 minutes*, one quadrupole doublet spectrum component could be identified with parameters typical for a high-spin Fe(III) with octahedral oxygen coordination. At the same time, the presence of signals associated with Fe(II) or magnetic components (hematite, goethite) could not be confirmed.

Upon the recovery treatment using NH particles, started at 9:00 am in the morning, the first sign of the recovery of iron deficiency symptomes was measured as a delayed diurnal increase in the expression of the ferric chelate reductase gene *CsFRO1*. The relative transcript amount of the ferric chelate reductase gene *CsFRO1* reached its peak and started to decrease from 19:00 pm and thus reduced to a minimum by 24:00 pm, and later remained in the range of the Fe(III)-EDTA supplied sufficient plants. Elimination of the iron deficiency induced expression of *CsFRO1* required 15 h in total from the beginning of the recovery treatment.

Similarly to *CsFRO1*, the relative transcript amount of *CsFRO3*, a secondary ferric chelate reductase gene, also decreased after 15 h of treatment. In contrast, decline in the relative transcript amount of *CsFRO2*, the third component of ferric chelate reductases of cucumber roots was delayed compared to that of *CsFRO1*&*CsFRO3*. The relative transcript amount of *CsFRO2* only decreases significantly after 48 h of treatment. The relative transcript amount of *CsRIBA1*, riboflavin biosynthesis component, decreased significantly to 24:00 midnight of the first day of treatment and becomes comparable to Fe sufficient control plants, similarly to that of the *CsFRO1*&*CsFRO3* expression. The ferric chelate reductase activity of the roots was first altered 24 hours after the initiation of the recovery treatment (9:00 am on the second day of treatment). Thus, the tendency of changes in the ferric chelate reductase activity apparently turned into a continuous decay. Finally, the ferric chelate reductase activity of the regenerated plants decreased to the level of the Fe(III)-EDTA supplied positive control plants at 9:00 am on the third day of treatment. Thus the recovery of the ferric chelate reductase activity showed in sum a delay in comparison to the relative transcript amount of *CsFRO1&3* and *CsRIBA1*, but was more coincidental with decrease of the relative transcript amount of *CsFRO2*.

In conclusion, the application of NH particles enabled the study of the restoration of iron deficiency responses. The slight decrease in the size of the particles accumulating in the root apoplast together with the changes in the Mössbauer parameters implicate a release of Fe from the nanoparticles, in which effect, together with a decreased nutrient solution acidification, apoplast flavins may play a role. The fast reaction in the relative transcript amount of some iron deficiency response genes also support the quick mobilisation of iron from the NH nanoparticles. Thus, stable NH nanoparticles can be considered as a perspective material for iron nutrition as well.

Testing manganese-zinc ferrite (MSZ26) nanoparticles as microelement fertilizers

Over NH, manganese-zinc ferrites were also considered being effective in supporting the iron nutrition of plants [15]. Based on the preliminary experiments, one of the major targets of our research was the nanoferrite MSZ26 with the nominal formula $Mn_{0.25}Zn_{0.75}Fe_2O_4$. We have evaluated its effects on cucumber model both as microelement donor (fertilizer) and a potentially toxic agent. The presence of nanoparticles in the MSZ26 suspension sample was also confirmed by Malvern nanoZetasizer analysis as the average particle size proved to be 4-7 nm after filtration. (The suspension was found to contain some particles of about 20 nm prior to filtration.) In order to assess the release of free ionic components from the metal containing nanoparticles the original MSZ26 colloid suspension was diluted in buffer solutions of MES (pH 5.0) and K_2CO_3:$KHCO_3$ (pH 7.5), and the resulted solutions were tested for sedimentation by high-speed centrifugation. Particle size analysis revealed that at pH 5 the supernatant of diluted MSZ26 suspensions did not contain any nanomaterial particles but components of subnanometer size. At pH 7.5 the supernatant contained particles of 5-6 nm. The element composition of MSZ26 nanoparticle suspension and the achieved supernatant was analysed by ICP-OES. Based on the results the molar ratio of Fe:Mn:Zn was calculated. The native composition of the MSZ26 was characterised with a molar ratio of approximately 8.5:1:3. The supernatant of the MSZ26 suspensions diluted with deionized water at both pH values had a markedly different molar ratio of (1.5-1.6):1:(1.1-1.3). When the soluble concentration of Fe, Mn and Zn was calculated in the treatment nutrient solution based on the concentration of metals in the supernatant, it was found that it was markedly lower for the specific metal the deficiency of which was studied, as compared to the pregrowth control solution at pH 5 and it further decreased at pH 7.5. The other metals were present in sufficient concentration. Results showed that MSZ26 is an iron containing nanomaterial with good solubility and high stability. The release of free ionic constituents from MSZ26 is low which suggests, on the one hand, that a transient supply of microelements to the roots can be expected and, on the other hand, that the uptake of metals from MSZ26 may occur in intact nanoparticulate form.

Regeneration of plants from microelement deficiency by MSZ26

To study the plant nutritional potential of MSZ26, cucumber plants were applied. To study the potential in the iron nutrition, plants were grown in iron-free nutrient solution for two weeks and then were transferred to 10 μM MSZ26 or Fe(III)-citrate (for comparison) containing nutrient solutions. After one week of regeneration the initial yellowish green leaves fully regreened independently of the applied Fe-source and their growth approached that of the plants supplied with Fe-citrate from the beginning of culture. To study the initial phase of regeneration, cucumber plants were grown for one week in nutrient solution containing (5 μM) Fe(III)-EDTA, then iron deficiency of the newly developing shoot parts was induced in the following two weeks in completely iron-free nutrient solution. Thereafter, plants were transferred again to a fresh solution containing a nominal concentration of 20 μM of MSZ26 as iron source. Physiological measurements were taken in the following 3 days. Treatments induced a small growth stimulation compared to the iron deficient control plants but the time frame was considered too short to achieve significant differences. However, the chlorophyll concentration of the third leaves increased by 135–168% and reached 50% of that measured in the other control grown in 10 μM Fe-EDTA over the whole period. The maximal quantum efficiency of photosystem II reaction centres (F_v/F_m) indicator of the status of the photosynthetic apparatus, has indeed increased up to the control level, from approx. 0.6 to 0.8.

The efficiency of the MSZ26 in supplying micronutrients was tested with cucumber model plants treated in slightly acidic (pH 5.2–5.5) and slightly alkaline pH (pH 7.5) range. At the acidic range no buffer was added to the nutrient solution so that its pH increased during the time of treatment in all cases except for that of plants grown under iron deficient („dFe") conditions where it decreased. The MSZ26 treatments did not cause significant changes in the pH compared to that of the untreated plants except for the dFe plants where the pH of the solution significantly increased. Treatments in the alkaline pH range did not change the solution pH significantly due to the applied buffer. The total dry weight of the iron deficient plants were significantly lower at both pH levels than that of the control, but it was not different for manganese deficient plants at alkaline pH. MSZ26 treatment increased the dry weight of all deficient plants at acidic pH, but the change was not significant compared to the untreated deficient plants. In case of manganese deficient plants, however, the total dry weight reached that of the sufficient control. At alkaline pH there was no significant change at all. The relative water content of plant tissues were not different from the control in any treatment except for iron deficient plants, both treated and untreated with MSZ26, where it was significantly lower. In contrast, in case of acidic pH it was increased significantly by MSZ26 treatment in iron deficient plants.

Changes in the pigment composition and functioning of the photosynthetic apparatus were assessed based on the chlorophyll concentration and ratio as well as excitation energy allocation in the second leaf. At acidic pH, the chlorophyll concentration was the highest in the control plants, but neither Mn and Zn deficiency treatments nor the correction by MSZ26 led to values significantly different from it. Iron deficiency markedly decreased the chlorophyll concentration, while MSZ26 treatment of iron deficient plants significantly increased it, though did not restore the control level. These findings were similar when the chlorophyll concentration was calculated for leaf fresh weight or surface area, but in manganese deficient and zinc deficient plants the chlorophyll concentration decreased somewhat under MSZ26 treatment, referring to a higher surface growth of the leaves at acidic pH. The chlorophyll concentration was lower at alkaline pH in the control and all deficiency treatments, and both on leaf fresh weight basis and surface area basis, except for iron deficient plants in which it was similar to corresponding values obtained for acidic pH. The chlorophyll a/b ratio significantly decreased in manganese deficient plants and significantly increased in iron deficient plants, but it was restored to control level by the MSZ26 treatment at both pH levels.

Physiological parameters related to photosynthetic capacity, such as the maximal quantum efficiency of photosystem II reaction centres (F_v/F_m), indicating the functioning of the photosynthetic apparatus, dependent on the transitional metal homeostasis of plants, did not change significantly in sufficient control plants at different pHs. Zn deficiency has no effect on this parameter but it significantly decreased under Mn and Fe deprivation compared to the control plants. MSZ26 treatment led to the total regeneration of F_v/F_m in manganese and iron deficient plants. Concerning the excitation energy allocation of the photosynthetic apparatus, indicating the details of the operation of the photosynthetic machinery, F_v/F_m significantly deceased in plants grown on slightly acidic pH on Fe-free or Mn-free

medium compared to the corresponding sufficient controls, whereas plants on Zn-free medium performed no alteration in the excitation energy allocation compared to the controls. MSZ26 treated plants showed a recovery in the actual quantum efficiency. In parallel, fluorescence and constitutive heat dissipation ($\Phi_{f,\ D}$) also recovered in MSZ26 treated plants. The excitation energy quenching in the antennae (Φ_{NPQ}) showed no change in any treatments compared to the corresponding control. However, the excitation energy quenching of the inactivated PSII reaction centres (Φ_{NF}) showed a significant increase under both Fe and Mn deficiency. Recovery treatment by MSZ26 induced a decrease in this parameter, too. At alkaline pH, the actual quantum efficiency of photosystem II reaction centres of plants grown under Fe and Mn-free conditions also decreased compared to the corresponding controls, whereas on Zn-free medium, plants did not show decrease. Regeneration induced by MSZ26 treatment proved to be successful, but quantum efficiency values did not recover completely: the actual quantum efficiency of regenerated plants remained significantly lower compared to the corresponding controls. The fluorescent and constitutive heat dissipation also increased significantly by the MSZ26 induced recovery. The antennae-based excitation energy quenching decreased significantly in plants grown either under Fe-free or Mn-free conditions compared to the corresponding controls. This quenching, indeed, was not recovered by the MSZ26 treatment later. In comparison, excitation energy quenching of the inactivated photosystem II reaction centres was also induced in plants grown under Fe-free or Mn-free condition, but it recovered upon the MSZ26 treatment.

In the experiment performed with unbuffered nutrient solutions, i.e. at slightly acidic pH, Mn concentration was significantly lower in manganese deficient plants than that of the control plants, and it markedly increased upon MSZ26 treatment. Nevertheless, the change was not statistically significant. Though Zn deprivation did not result in the expected Zn deficiency, and thus the Zn concentration in the second leaves of plants was not significantly different from that of the sufficient control, Zn concentration almost doubled due to MSZ26 treatment. Fe deprivation resulted in a significant decrease in Fe concentration of the second leaf compared to that of sufficient control plants. Under MSZ26 treatment of iron deficient plants Fe concentration has increased considerably, and in 3 days it reached a value twice as high as in the sufficient control. Mn and Zn concentration in iron deficient plants was elevated compared to control plants, and after MSZ26 treatment the concentration of Mn decreased significantly but that of Zn did not change. Similarly, the concentration of Fe and Zn was increased in manganese deficient plants as compared to the control ones, and the latter was statistically significant. MSZ26 treatment did not cause further changes in these plants. Fe and Mn concentrations did not change significantly either in Zn deprived plants or after MSZ26 treatment as compared to the sufficient control.

At alkaline pH there was no marked change in the element distribution as compared to the case of acidic pH. Fe concentration did not increase but decreased in the second leaves of manganese deficient plants compared to the control. In Zn-deprived plants Zn concentration significantly decreased compared to the control, whereas in iron deficient plants Zn did not increase like in the plants grown at acidic pH.

These results show that at the acidic pH range MSZ26 can be an efficient fertilizer for Fe and Mn, but its fertilizer properties proved to be insignificant as Zn source. At alkaline pH MSZ26 failed to efficiently regenerate microelement deficiency in cucumber.

Mechanism of utilization of micronutrients from MSZ26

Ferric chelate reductase activity of the roots of cucumber model plants growing in iron deficient conditions was tested at pH 6 and pH 8 and in the presence of Fe(III)-EDTA (for comparison) and MSZ26 as substrates. Furthermore, ferric chelate reductase activity was also investigated after MSZ26 pretreatment in the presence of Fe(III)-EDTA. At pH 6 ferric chelate reductase activity with Fe-EDTA was significantly higher (101.410±25.048 nmol Fe g^{-1} root fw min^{-1}) than at pH 8 (35.575±5.235 nmol Fe g^{-1} root fw min^{-1}) but MSZ26 failed to serve as substrate for reduction at both pHs. However, after a 3-hour MSZ26 pretreatment the ferric chelate reductase activity with Fe(III)-EDTA decreased a little, the change became significant only after a week pretreatment though. (15.3±14.7 nmol Fe g^{-1} root fw min^{-1})

Images taken of ultrathin sections of root tips by TEM did not reveal any accumulation of MSZ26 in the apoplastic or symplastic spaces. The xylem sap of the plants was collected after decapitation of 3 week-old plants which were

pregrown on 5 µM Fe(III)-EDTA on the first week then further grown on dFe nutrient solution and control ones. The nutrient solution at decapitation contained either Fe(III)-EDTA or MSZ26, and thus a total of four treatments were applied: oFe/Fe(III)-EDTA, oFe/MSZ26, dFe/Fe(III)-EDTA dFe/MSZ26, where oFe stands for Fe-supplied and dFe for iron deficient treatments. Based on ICP-OES data, the iron deficient plants resupplied with Fe(III)-EDTA transported more than twice as much Fe in the xylem sap compared to plants grown on optimal Fe (oFe). Similarly, in the dFe plants supplied with MSZ26 the Fe concentration in the sap increased compared to oFe plants, but only by 14%. The Fe concentration in the xylem sap of dFe/MSZ26 plants was just 41% of dFe/Fe(III)-EDTA ones. The Mn concentrations in the xylem sap were very similar in dFe plants at both treatments. It increased in oFe/Fe(III)-EDTA and oFe/MSZ26 by 10 and 18%, respectively. Zn concentrations were also similar in dFe plants but changed in the opposite way: it decreased in oFe/Fe(III)-EDTA and oFe/MSZ26 plants by 44 and 46%, respectively.

The typical bright field TEM images taken from the xylem sap sample of oFe/MSZ26 plants did not reveal the presence of MSZ26 nanoparticles. Samples from dFe/MSZ26 plants were also studied and the results were similar to the previous one. Selected area electron diffraction (SAED) pattern indicated the presence of nanocrystals in the imaged area. The most intense diffraction ring, characteristic of the nanocrystals was at ca. 28 nm. The largest crystals were about 5 nm in size, and besides them a large number of smaller crystals with size on the 10 nm scale could be observed. EDS measurements indicated that the main components in these nanocrystalline areas are Ca, O, C, and besides that, low amount of Si, P, Mg, K, S and Cl are present. Based on the major elements detected in EDS spectrum, and the diffraction ring at ca. 28 nm, the nanocrystals are supposed to be cubic CaO, which might form from oxalates under the electron beam.

Wide range X-band EPR spectra, recorded of the frozen xylem fluid samples at 150 K, revealed two different signal ranges: the central (ca. 3-4 kG) applied field range were occupied mainly by the EPR signal of paramagnetic Mn^{2+} species, whereas at around 1500 G a smaller peak associated with paramagnetic Fe^{3+} (S = 5/2) species was seen. The latter can be associated with Fe^{3+} complexes where iron experiences ligand fields of mainly rhombic symmetry. Comparing the respective amplitudes of the Fe^{3+} and Mn^{2+} signals associated with the different samples, we found fair qualitative correlation with the corresponding ICP-OES data related to the total Fe and Mn concentrations: dFe-based samples displayed higher Fe^{3+} and lower Mn^{2+} signal amplitudes than oFe-based ones. In order to investigate the Mn^{2+} signal in more detail, the spectra were also measured with an increased resolution in the central region. The shape of the Mn^{2+} signal agrees quite well across the four samples, suggesting that they refer to the same Mn^{2+} species in each of the studied xylem fluids. The Mn^{2+} signal in question bears close similarity with that of $Mn^{2+}(H_2O)_6$ in frozen solutions, which was confirmed by further analysis of the spectra. The signal associated with paramagnetic Fe^{3+} ions (at $B \approx 1500$ G) displays higher amplitude in the samples originating from plants grown under dFe conditions than in those associated with oFe conditions, in agreement with ICP-OES data. However, the samples may contain iron in EPR-silent forms as well: antiferromagnetically coupled dimer species of Fe^{3+}, for example, could have remained undetected in the EPR spectra. To check for the presence of a possible EPR-silent species in the samples, the original xylem fluids were measured again after administration of different amounts of H_2O_2 in order to transform EPR silent components to EPR detectable Fe^{3+} monomers by achieving, e.g., separation of Fe^{3+} dimers. The administration of H_2O_2 to the xylem fluids resulted in a significant increase in the amplitude of the Fe^{3+} EPR signal in all the four cases, suggesting that in the original frozen xylem fluid samples a large fraction of iron was present as EPR silent iron species.

These results show that MSZ26 is not taken up and transported to the shoot in cucumber plants. Instead, MSZ26 may be adsorbed to root surfaces and in the cortical apoplast, and the regeneration of plants from microelement deficiency is resulted by the slow release of ionic constituents that are utilized by the roots. This stability of MSZ26 is underlined by the root ferric chelate reductase reactions in which no Fe^{2+} release was experienced referring to the efficient coating.

The effect of MSZ26 on seed germination

We have conducted a germination test with cucumber model for evaluating the effect of MSZ26. We have placed 50 seeds in Petri dishes (d = 13.5 cm) in 3 parallel on filter paper disk moistened with 16 ml nanomaterial suspensions in dark thermostat set to 30 °C for two days. It was found that MSZ26 stimulated germination at all the three applied

concentrations (0.01; 0.1 and 1.0 mM) and the fresh weight of the germinating seeds was also significantly higher. The root length gradually increased with increasing concentration but was significantly higher compared to the control at 1 mM MSZ26. Based on these findings MSZ26 may be applied for seed coating.

Other essential heavy metal containing nanoparticles as potential Fe fertilizers

Dissolution of manufactured magnetite (Figure 2) and zinc-ferrite [9] nanocolloid suspensions (nanomagnetites MG001 and MG002, Zn-ferrites ZnFe001 and ZnFe002) was investigated in the frame of a high-speed centrifugation pelleting experiment on pH 5.0 and pH 8.5, in the presence of buffers and different concentrations of riboflavin, root exudate of Strategy I model plant cucumber. Fe concentration of the supernatant was under 0.005% of the original Fe content of all samples. Conversely, dissolution of Zn at low pH (pH 5.0) was significant (22.85%) in case of Zn-containing nanomaterials (ZnFe001 and ZnFe002). Riboflavin concentration increased the dissolution of Zn but it had no effect on Fe dissolution.

As searching for further potential iron containing nanomaterials in iron nutrition, screening of 6 nanomaterials MG001, MG002, ZnFe001, ZnFe002, paper-bound Fe/FeO nanoparticles ("Fe-EWE-2018/S", Figure 3b) and the suspension "Fe-EWE 2018/F" were investigated on cucumber. Three of the nanomaterials (MG001, MG002 and "Fe-EWE-2018/S" paper-bound Fe/FeO nanoparticles) were able to successfully regenerate Fe deficiency including 2-3 fold increase in Chl content, fresh and dry weight and increase in medium pH within 3–7 days during treatment, showing potential as Fe fertilizers.

To study the presence of the manufactured nanomaterials in the xylem sap of cucumber model plants, 3-week-old plants grown on optimal Fe (oFe) or in Fe deficient condition (dFe), MG001 and Fe(III)-EDTA were applied at 100 µM concentration with respect to Fe. The plants were decapitated and the xylem sap was collected for 30 min. As revealed by ICP-OES, the concentration of Fe in the collected sap samples decreased in the order of oFe/FeEDTA (0.331 mg/L), dFe/FeEDTA (0.304 mg/L), dFe/MG001 (0.278 mg/L). This confirms that nanomagnetite may sufficiently supply Fe to plants, even though it may not be transported to the shoot as nanomaterial.

Application of MSZ26 and Fe-oxide nanoparticles "Fe-EWE 2018/F" as foliar fertilisers

Regeneration of iron deficient cabbage (*Brassica oleracea* L. convar. *capitata* var. *alba*) model system was investigated in foliar treatments application of MSZ26 and the suspension "Fe-EWE 2018/F". Nutrient solution grown plants were pre-cultivated on 10 µM Fe then transferred to iron-free medium containing $CaCO_3$. Following 3 weeks of treatment, leaves developed under iron deficiency were subjected to foliar treatment: Fe(III)-citrate (20 µM, 2 mM, 5 mM, 10 mM), MSZ26 (0.2–2–5–20 mM), "Fe-EWE 2018/F" (1 µM - concentration of the stock solution). 200 µL solution containing 0.1% nonite surfactant was applied on both sides of leaves. Physiological recovery was followed by leaf chlorophyll content. 5 mM Fe(III)-citrate and MSZ26 treatment caused significant changes (SPAD values were 29.5±4.9 and 10.1±2.7, respectively) compared to iron deficient control (2.3±0.6). However, "Fe-EWE 2018/F" was ineffective, and after repeating the experiment several times, MSZ26 was subsequently not found to be effective in recovery, either.

Effect of nanoparticles applied in toxic concentration range on plants

Non-essential metal containing nanomaterials "ALH" and „nanoTiO_2"

Non-essential metal containing nanoparticles—that may appear in the environment—may have toxic effects among others on plants. On the other hand, the same nanomaterial particles could also play a role as protective compounds against various biotic and abiotic stress factors. To assess their potential toxic effects, we have conducted germination tests with white mustard (*Sinapis alba* L.) using suspensions of nanometric TiO_2 ("nanoTiO_2") and aluminium-hydroxide ("ALH"). The germination test was terminated on the 5^{th} day. The nanomaterial concentration was 0.01; 0.1 and 1.0 mM. The tests showed that neither ALH at any concentrations, nor nanoTiO_2 at 0.01 and 0.1 mM had significant effect. At the same time, nanoTiO_2 significantly increased germination (%) at 1 mM concentration. The root and shoot length was increased at all treatments by the applied nanomaterials but the difference compared to the control was not significant.

We also investigated the effects of nanoTiO_2 in excessive concentrations (10 µM, 100 µM and 1 mM) on cucumber and wheat model plants [16]. While the dry weight of plants did not increase significantly at 10 µM, it did increase significantly at the 100 µM nanoTiO_2 containing nutrient solution. Only the highest concentration inhibited growth of cucumber significantly. Transpiration decreased with the increasing concentration. Toxicity symptoms were evaluated based on the adjacent oxidative stress arose in parallel to the application of the nanomaterial. Result of Lipid peroxidation measured as malondialdehyde content in the shoots, whereas superoxide dismutase activity decreased at the highest applied nanoTiO_2 concentration. At lower concentration we found increased superoxide dismutase activity. In comparison, wheat showed to be highly resistant to the treatments, and showed no significant effects.

Non-essential zero valent heavy metal containing nanomaterial "nanoFeCo"

To assess the potential toxic effects of zero valent heavy metal containing nanomaterial particles, nanoFeCo was tested at 0.1 mM and at 1 mM concentration on cucumber model plants, applied in nutrient solution [17]. Nanomaterial particles were supplied to the nutrient solution after 1 week pregrowth, which contained 10 µM Fe(III)-citrate over the Fe content of the nanomaterials. The effect of treatments was measured in two weeks. The nanoFeCo alloy caused 70 and 90% inhibition in 0.1 and 1 mM concentration, respectively. Stomatal conductance of the leaves, indicating toxicity syndrome, changed similarly: treatment with nanoFeCo caused a significant, 70% inhibition, in both concentrations. The chlorophyll contents of the leaves also decreased by more than 90% compared to the untreated control. The inhibitory effect was coupled with the 50-70% decrease in Fe concentration and a highly significant Co accumulation in the 2nd leaves of the plants (only two leaves have developed). (The Co concentration was 168 ppm and 324 ppm at 0.1 and 1 mM nanoFeCo, respectively. The Co content was less than 1 ppm in the control plants.)

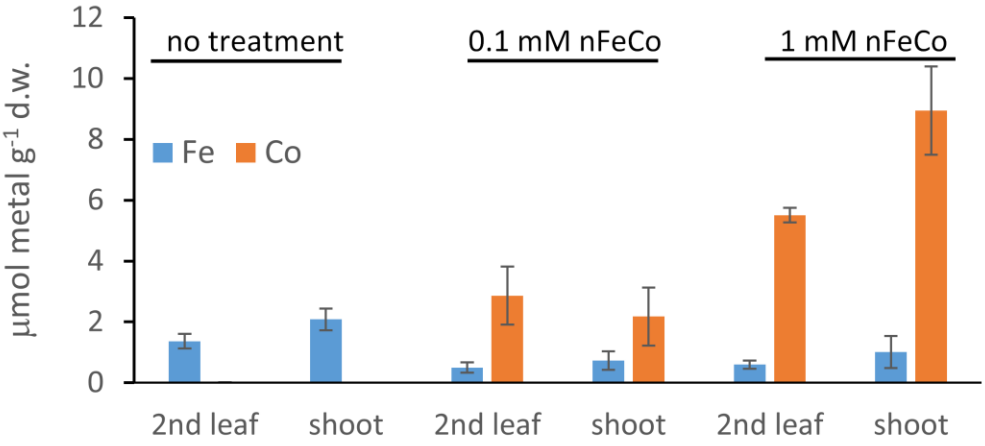

Figure 4. Fe and Co accumulation in zero valent nanoFeCo alloy treated cucumber plants. Note the decrease in the Fe content of the treated plants accompanying the accumulation of Co in their 2nd leaf and shoot.

The toxic effect of 100 µM and 1 mM nanoFeCo was also compared to the non-nanometric, zerovalent Fe and zerovalent Co particles in same concentration added either separately or together to the nutrient solution of cucumber model plants. The plants treated with nanoFeCo showed less toxicity than the ones treated in the same concentrations with zerovalent Co. The nanoFeCo changed the root morphology of the cucumber model. The presence of nanoFeCo induced secondary root growth exactly on the tips of the roots at both concentrations. In comparison, 100 µM zerovalent Co caused shortening, while 1 mM totally damaged the roots. To study the release of metals from FeCo nanoparticles, high-speed centrifugation was applied on Hoagland's nutrient solution containing the nanomaterial particles, and subsequently the metal content of the supernatant was determined by ICP-OES. Co content of the supernatant was one tenth and one fifth compared to nutrient solutions containing zerovalent Co at 100 µM and 1 mM concentration, respectively. Based on these observations the nanoFeCo alloy is a less toxic material as compared to non-nanometric Co, but causes growth retardation and deformation as well as inhibition of Fe uptake/translocation, thus it is an environmentally hazardous material.

Essential metal containing nanomaterial particles

To assess the potential toxic effects of essential heavy metal containing nanomaterial particles, nanoparticle suspensions of MSZ26 and FH were applied in 0.1 mM concentration on cucumber model, in hydroponics. The effect of treatments was measured in two weeks. None of the nanomaterials tested caused growth inhibition. The Fe concentration of the 3rd leaves of the plant model did not change significantly when 0.1 mM MSZ26, or FH was applied. But the Mn concentration increased almost 8-fold and the Zn concentration increased 3-fold by the effect of MSZ26. This increase in the microelement concentration of the leaves does not result in measurable physiological changes.

MSZ26 was also applied in toxicity experiments, when its Fe content was in the supraoptimal range (equivalent with 1 mM of Fe, i.e. hundred-times the Fe concentration applied in the case of the control) in the nutrient solution of cucumber plants. It hindered plant growth and resulted in reduced plant fresh weight. At the same time, applying the same amounts of Mn, Zn and Fe in the form of a mixture of iron citrate, $MnCl_2 \cdot 4H_2O$ and $ZnSO_4 \cdot 7H_2O$ inhibited plant growth in a greatly enhanced manner in comparison, revealing the considerably less toxic nature of metals when administered in the form of the MSZ26 nanoparticles. This result points out that nanoparticles may act as a retarded (and consequently prolonged) source of metals, by providing access to their metal content solely through their cumulative surface area.

Some of the experiments were repeated with 0.1 and 1 mM MSZ26 and FH applied to wheat (*Triticum aestivum* L. cv. MV Tallér) which proved to be less sensitive to heavy metal stress. FH nanoparticles only in 1 mM concentration triggered decrease in transpiration and increase in root lipid peroxidation (malondialdehyde content) revealing the harmful effect of extreme doses.

Potential fungicid activity of MSZ26 on powdery mildew sensitive wheat

Wheat plants (powdery mildew sensitive, *Triticum aestivum* L. cv. Carsten) were grown in quarter-strength Hoagland's solution for three weeks. Wheat plants were inoculated with the powdery mildew strain '76' and upon the first visible signs of the infection, MSZ26 suspension (0.01 µM) with nonite adjuvant (0.01%) was sprayed on the leaf surface of the infected plants. After one week, the status of the photosynthetic apparatus was measured by chlorophyll *a* fluorescence induction. Excitation energy allocation of the infected plants changed fundamentally: together with the increase in the excitation energy quenching of the non-functional photosystem II reaction centres, the non-photochemical quenching of the antennae and the photochemical efficiency of PSII reaction centres decreased compared to the non-treated control. The application of MSZ26 caused no significant increase in the PSII photochemical efficiency. However, the treatment decreased the inactivation-based quenching (0.292±0.025 versus 0.211±0.079, respectively) and increased the antennae-based quenching (0.375±0.095 versus 0.412±0.029) in comparison to the untreated infected plants. Thus, the zinc-containing MSZ26 proved to be a candidate fungicide or fungistatic compound. Nevertheless, the powdery mildew infection was too much serious under controlled environment, thus further investigations are needed to prove the efficiency of MSZ26.

Essential heavy metal containing nanomaterials as potential growth enhancers

Open field experiments started in 2018. At ELTE Füvészkert 'Huzella Kert' (Göd) a 60 m^2 sandy field was trenched and a total of about 18 m^2 was planted with a powdery mildew sensitive wheat variety previously applied in hydroponic experiments (*Triticum aestivum* L. cv. Carsten). In this open field soil culture, wheat plants were infected by naturally occurring powdery mildew strains. The culture was treated by nanoTiO_2 and MSZ26 when the flag leaf of the plants appeared (April, 2018). In a month time, excitation energy allocation, transpiration and relative chlorophyll density were recorded on the flag leaves, as parameters sensitive to the fitness of the plants and indicators of plant health. Both nanoTiO_2 and MSZ26 treatments increased the photochemical efficiency of photosystem II reaction centres in comparison to the untreated infected plants (values were: 0.184±0.067; 0.262±0.015; 0.118±0.005, respectively). The treatment with nanoTiO_2 also contributed to the increase in the transpiration rate (values of the nanoTiO_2, MSZ26 treated and untreated infected plants were: 219.4±80.9; 166.8±34.0; 176.4±53.6 mmol H_2O m^{-2} s^{-1}, respectively). The positive effect of the nanomaterials could also be detected in the SPAD indexes (relative chlorophyll density): it was:

48.9±4.5; 49.5±3.0 and 47.4±2.6 in nanoTiO_2, MSZ26 treated and untreated infected plants, respectively. A positive effect was also detected in the average yield of the plants: the average grain weight was: 22±5 mg; 24±0 mg and 20±7 mg in nanoTiO_2, MSZ26 treated and untreated infected plants, respectively, whereas no differences were found in the average spike number per plants and average sum grain weight in spikes. Between April 10 and May 1, both in 2019 and 2020, the foliar spray treatments were repeated four times before, during and after the development of the generative tissues. NanoTiO_2 and MSZ26 were applied in 6 parallel. Being a sensitive cultivar, the plants were naturally infected by powdery mildew.

Though laboratory tests and the first year open field experiment suggested that nanomaterial treatment could improve the tolerance against powdery mildew infection, the applied treatments neither stopped powdery mildew colonisation nor did stimulate the growth and chlorophyll accumulation of the plants. Thus, nanoTiO_2 and MSZ26 was considered not quite effective in enhancing plant growth in powdery mildew sensitive wheat. Indeed we have to underline, that due to meteorological situations, the natural powdery mildew infection also remained below the threshold in the untreated plants as well.

References

[1] Z. Klencsár, P. Németh, Z. Sándor, T. Horváth, I.E. Sajó, S. Mészáros, J. Mantilla, J.A.H. Coaquira, V.K. Garg, E. Kuzmann, Gy. Tolnai: Structure and magnetism of Fe-Co alloy nanoparticles, *Journal of Alloys and Compounds* **674** (2016) 153. (DOI: 10.1016/j.jallcom.2016.03.068)

[2] Z. Klencsár, V.K. Kis, S. Stichleutner, Z. May, Z. Sándor, E.Gy. Szabó, E. Bódis, L. Szabó, K. Kovács, E. Kuzmann, Z. Homonnay, F. Pankaczi, Zs. Farkas, Á. Solti, F. Fodor, Gy. Tolnai: *Nanoparticle systems developed for plant nutrition: their composition, structure and effects on cucumber plants*, Booklet Abstracts p. 83, *The International Conference On Functional Nanomaterials and Nanodevices*, September 24-27, 2017, Budapest, Hungary, ISBN 978-954-2987-31-4, 2017.

[3] Z. Homonnay, Gy. Tolnai, F. Fodor, Á. Solti, K. Kovács, E. Kuzmann, A. Ábrahám, E.Gy. Szabó, P. Németh, L. Szabó, Z. Klencsár: Iron oxide nanoparticles for plant nutrition? A preliminary Mössbauer study, *Hyperfine Interactions* **237** (2016) 127. (DOI: 10.1007/s10751-016-1334-1)

[4] S.W. da Silva, L.R. Guilherme, A.C. de Oliveira, V.K. Garg, P.A.M. Rodrigues, J.A.H. Coaquira, Q. da Silva Ferreira, G.H.F. de Melo, A. Lengyel, R. Szalay, Z. Homonnay, Z. Klencsár, Gy. Tolnai, E. Kuzmann: Mössbauer and Raman spectroscopic study of oxidation and reduction of iron oxide nanoparticles promoted by various carboxylic acid layers, *Journal of Radioanalytical and Nuclear Chemistry* **312**(1) (2017) 111-119. (DOI: 10.1007/s10967-017-5195-0)

[5] A. Lengyel, Z. Homonnay, K. Kovács, Z. Klencsár, S. Németh, R. Szalay, V. Kis, F. Fodor, Á. Solti, M. Ristic, S. Music, E. Kuzmann: Characterization of nanomagnetites co-precipitated in inert gas atmosphere for plant nutrition, *Hyperfine Interactions* **239** (2018) 38. (DOI: 10.1007/s10751-018-1516-0)

[6] A. Lengyel, Gy. Tolnai, Z. Klencsár, V.K. Garg, A.C. de Oliveira, L. Herojit Singh, Z. Homonnay, R. Szalay, P. Németh, B. Szabolcs, M. Ristic, S. Music, E. Kuzmann: The effect of carboxylic acids on the oxidation of coated iron oxide nanoparticles, *Journal of Nanoparticle Research* **20**(5) (2018) 137. (DOI: 10.1007/s11051-018-4247-x)

[7] A. Lengyel, V.K. Garg, A.C. de Oliveira, S.W. da Silva, L.R. Guilherme, Z. Klencsár, Z. Homonnay, J.A.H. Coaquira, Gy. Tolnai, E. Kuzmann: Mössbauer spectroscopy control of the preparation of citric- and mandelic acid functionalized nanomagnetites, *Hyperfine Interactions* **239** (2018) 17. (DOI: 10.1007/s10751-018-1493-3)

[8] Z. Klencsár, A. Ábrahám, L. Szabó, E.G. Szabó, S. Stichleutner, E. Kuzmann, Z. Homonnay, Gy. Tolnai: The effect of preparation conditions on magnetite nanoparticles obtained via chemical co-precipitation, *Materials Chemistry and Physics* **223** (2019) 122-132. (DOI: 10.1016/j.matchemphys.2018.10.049)

[9] Z. Klencsár, K.V. Kovács, S. Stichleutner, Z. May, E. Kuzmann, L.K. Varga, L.F. Kiss, D.L. Nagy, Gy. Tolnai: $ZnFe_2O_4$ Nanoparticles With Different Crystallinity: A Comparative Study, *International Conference on the Applications of the Mossbauer Effect (ICAME 2019)*, 01-06 September, 2019, Dalian, China, Conference Program p. 148, 2019.

[10] K. Lázár, L.K. Varga, V. Kovács Kis, T. Fekete, Z. Klencsár, S. Stichleutner, L. Szabó, I. Harsányi: Electric explosion of steel wires for production of nanoparticles: Reactions with the liquid media, *Journal of Alloys and Compounds* **763** (2018) 759-770. (DOI: 10.1016/j.jallcom.2018.05.326)

[11] Z. Klencsár, Gy. Tolnai, L. Korecz, I. Sajó, P. Németh, J. Osán, S. Mészáros, E. Kuzmann: Cation distribution and related properties of $Mn_xZn_{1-x}Fe_2O_4$ spinel nanoparticles, *Solid State Sciences* **24** (2013) 90. (DOI: 10.1016/j.solidstatesciences.2013.07.010)

[12] I.V. Alenkina, V. Kovács Kis, I. Felner, E. Kuzmann, Z. Klencsár, M.I. Oshtrakh: Structural and magnetic study of the iron cores in iron(III)-polymaltose pharmaceutical ferritin analogue Ferrifol®, *Journal of Inorganic Biochemistry* (2020) 111202. (DOI: 10.1016/j.jinorgbio.2020.111202)

[13] K. Kovács, J. Pechoušek, L. Machala, R. Zbořil, Z. Klencsár, Á. Solti, B. Tóth, B. Müller, H.D. Pham, Z. Kristóf, F. Fodor: Revisiting the iron pools in cucumber roots: identification and localization, *Planta* **244** (2016) 167-179. (DOI: 10.1007/s00425-016-2502-x)

Works submitted or in preparation

[14] A. Singh, M. Gracheva, V. Kovács Kis, Á. Keresztes, Z. May, M. Sági-Kazár, W. Ahmad, F. Pankaczi, B. Müller, K. Kovács, Gy. Tolnai, Z. Homonnay, F. Fodor, Z. Klencsár, Á. Solti: Utilisation of hematite nanoparticles by the roots of Cucumis sativus. Submitted to *Physiologia Plantarum* (PPL-2021-00055)

[15] A. Singh, F. Pankaczi, F. Farkas, B. Müller, Z. May, K. Solymosi, Z. Homonnay, E. Kuzmann, L. Szabó, Gy. Tolnai, Z. Szalai, K. Kovács, V. Kovács Kis, Z. Klencsár, Á. Solti, F. Fodor: Colloid suspension of coated Mn-Zn-ferrite nanoparticles regenerates Fe and Mn deficiency in cucumber in slightly acidic nutrient solutions. *In preparation/for Planta.*

[16] P. Pankaczi, B. Müller, Z. May, Z. Homonnay, E. Kuzmann, L. Szabó, T. Tolnai, K. Kovács, V. Kovács Kis, Z. Klencsár, Á. Solti, F. Fodor: Effect of nanoTiO_2 colloid suspension on growth and antioxidant defence in cucumber and wheat. *In preparation/for Plant Physiology and Biochemistry*

[17] F. Pankaczi, Z. May, K. Solymosi, Á. Keresztes, Z. Homonnay, E. Kuzmann, L. Szabó, Gy. Tolnai, K. Kovács, V. Kovács Kis, Z. Klencsár, Á. Solti, F. Fodor: Zero valent FeCo nanoparticles induce complex toxicity and iron deficiency syndrome in cucumber. *In preparation/for Environmental and Experimental Botany*